ELSEVIER

International Journal of Mass Spectrometry 209 (2001) 57–67

International Journal of Mass Spectrometry

# Useful yields of $MCs^+$ and $MCs_2^+$ clusters: a comparative study between the Cameca IMS 4f and the Cation Mass Spectrometer

T.Wirtz[a,*], B. Duez[a], H.-N. Migeon[a], H. Scherrer[b]

[a]*Laboratoire d'Analyse des Matériaux, CRP - Gabriel Lippmann, 162A, av. de la Faïencerie, L-1511 Luxembourg*
[b]*Laboratoire de Physique des Matériaux, Ecole des Mines, Parc de Saurupt, F-54042 Nancy Cedex, France*

Received 29 March 2001; accepted 18 May 2001

**Abstract**

The useful yields of $MCs^+$ and $MCs_2^+$ clusters strongly depend on the stationary cesium surface concentration $c_{Cs}$ incorporated in the specimen during the primary bombardment. The Cation Mass Spectrometer (CMS) has been designed to reach high $MCs_x^+$ useful yields by allowing an optimization of $c_{Cs}$ in an instrument providing a high transmission via a high extraction field and a magnetic sector spectrometer. For this purpose the CMS instrument has been equipped by several newly developed features, among which figures a sample stage and adapted collection optics allowing variations of the impact angle of the primary beam on the specimen at a constant primary energy. These variations of the incidence angle imply changes of the sputtering yield Y, which determines the Cs surface concentration according to $c_{Cs} = 1/(1 + Y)$. In this paper, we will study the improvement of secondary yields obtained on the CMS, in comparison with a classical Cameca IMS 4f, by making use of precisely this possibility to vary the sputtering yield. On both machines, analyses were performed on six different elements (B, F, Mg, S, As, and In) implanted in silicon samples. The observed variations of the useful yields are discussed in terms of the stationary cesium surface concentration incorporated in the specimen during the primary bombardment. Depending on the element, useful yield enhancements ranging from a factor 7 to a factor 80 can be observed between the CMS and the Cameca IMS 4f. This finding can be explained by the fact that the CMS allows to reach lower stationary Cs surface concentrations, which are close to the optimum value for the investigated samples. (Int J Mass Spectrom 209 (2001) 57–67)


*Keywords:* Secondary ion mass spectrometry; Quantification; Cesium clusters; Useful yield; Stationary cesium surface concentration

## 1. Introduction

Because of its low detection limits and high dynamic range, secondary ion mass spectrometry (SIMS) is a very sensitive technique for surface and thin-film characterization. To reduce quantification problems caused by the strong dependence of the ionization probability of the secondary ions on the sample composition ("matrix effect") [1], SIMS analyses are often performed by bombarding the sample with $Cs^+$ ions and detecting $MCs^+$ clusters [2–6] and $MCs_2^+$ clusters [7,8] in the case of electronegative elements, M being the element to be analyzed. The quantitative potential of this method is understood assuming that the $MCs^+$ ions are generated by the

* Corresponding author. E-mail: wirtzt@crpgl.lu


*PII* S1387-3806(01)00467-5

combination of a secondary neutral $M^0$ with a resputtered $Cs^+$ ion in the near surface region of the surface [3,5,9]. Consequently, the emission process for the species M is decoupled from the subsequent $MCs^+$ ion formation process in analogy to the ion formation in secondary neutral mass spectrometry resulting in a drastic decrease of the matrix effect.

It has been shown that the $MCs^+$ and $MCs_2^+$ yields strongly depend on the stationary cesium surface concentration incorporated in the specimen during the primary bombardment. An increasing Cs surface concentration can lower the electron work function below a critical value, which is situated slightly below the ionization energy of Cs. If this occurs, according to the electron tunneling model for secondary ion formation, the probability of secondary $Cs^+$ ionization and consequently the probability of $MCs^+$ and $MCs_2^+$ cluster formation strongly decreases [4,10–14].

The analysis of $MCs_x^+$ clusters is currently performed using dynamic SIMS instruments equipped with a primary ion column delivering $Cs^+$ ions in order to incorporate Cs into the specimen. The Cs surface concentration in the sample is determined by the primary bombarding conditions (mainly the impact energy and the incidence angle) which yield a distinct total sputtering yield Y and consequently determine the cesium surface concentration $c_{Cs}$ according to $c_{Cs} = 1/(1 + Y)$. It is however not likely that this, bombarding determined, Cs surface concentration is equal to the optimum concentration for highest $MCs_x^+$ yields.

The (Cation Mass Spectrometer) instrument, which is currently under development in the Laboratoire d'Analyse des Matériaux, has been designed to optimize the analysis of these $MCs^+$ and $MCs_2^+$ clusters [15]. The CMS machine should lead to high $MCs^+$ and $MCs_2^+$ useful yields by allowing to reach an optimum value of the mentioned stationary Cs surface concentration while keeping the high transmission tied to the use of a double focusing magnetic sector spectrometer.

For this purpose the CMS instrument has been equipped by several newly developed features:

1. Two primary ion guns delivering $Cs^+$ and $Ga^+$ focused ion beams respectively and which can be operated simultaneously in order to adjust the Cs proportion of the primary bombardment

2. A column delivering an adjustable flux of neutral Cs which can be used with either (or both) of the two mentioned ion guns

3. A sample stage and adapted collection optics allowing variations of the impact angle of the primary beam on the specimen at a constant primary energy. These variations of the incidence angle imply changes of the sputtering yield Y, which determines the Cs surface concentration according to $c_{Cs} = 1/(1 + Y)$.

In this paper we will study the improvement of useful yields of $MCs_x^+$ clusters obtained on the CMS instrument, in comparison with a classical Cameca IMS 4f, by making use of precisely this possibility to vary the sputtering yield. On both machines, analyses were performed at various sputtering yields on 6 different elements (B, F, Mg, S, As, and In) implanted in silicon samples. The observed variations of the useful yields are discussed in terms of the stationary cesium surface concentration incorporated in the specimen during the primary bombardment.

## 2. Experimental

A first description of the CMS instrument (Fig. 1) and some preliminary results regarding the secondary column and the surface ionization cesium gun have already been published elsewhere [15].

The CMS instrument offers the possibility to work at sputtering yields which can be varied over a large scale while bombarding the sample with $Cs^+$ primary ions. This is due to the combination of two facts. On the one hand the $Cs^+$ column is mounted on the main chamber at a relative large angle of 45° with respect to the normal to the sample stage. The combination between this geometric configuration and the deviation effects exercised on the primary ions by the extraction potential applied to the sample results in a large incidence angle of the primary beam on the sample. On the other hand, using the z motion of the sample stage to change the distance d between the sample surface and the extraction nose while keeping the primary energy constant can easily provoke

1 : Field emission Ga source
2 : Wien filter
3 : Surface ionization Cs source
4 : Electron gun
5 : Cs neutral gun
6 : Obturator system
7 : Sample
8 : Extraction-immersion lens
9 : Dynamic transferplates
10 : Transfer lens
11 : Contrast aperture
12 : Entrance slit
13 : Field aperture
14 : Electrostatic analyzer
15 : Energy slit
16 : Spectrometer lens
17 : Electromagnet
18 : Exit slit
19 : Projector lenses
20 : Electrostatic analyzer
21 : Electron multiplier
22 : Faraday cup
23 : Channel plate
24 : Fluorescent screen
25 : CCD camera
26 : Airlock
27 : Quartz microbalance

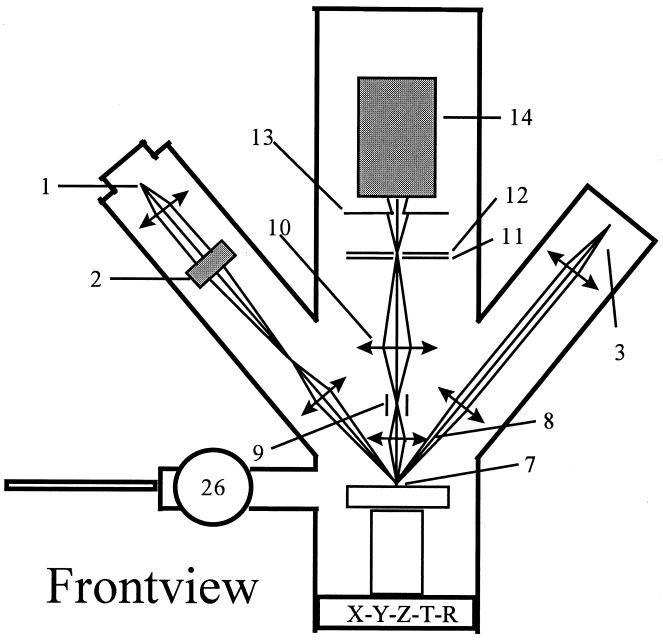


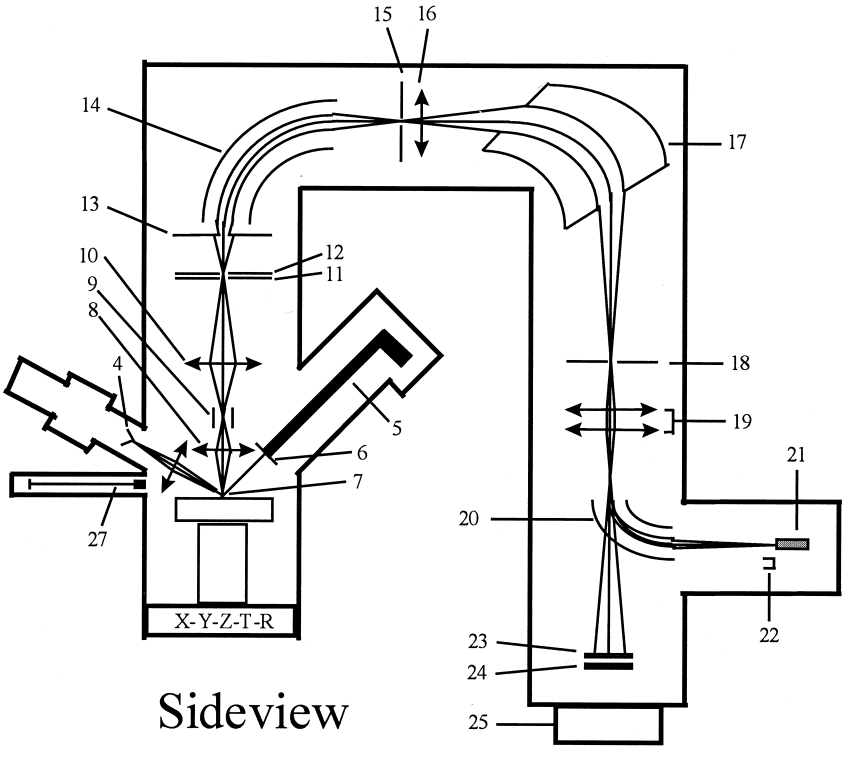


Fig. 1. Schematic representation of the CMS instrument.

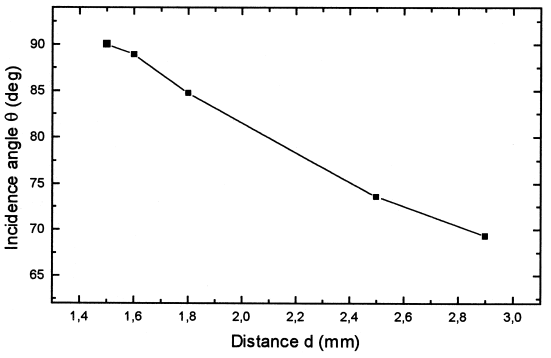


Fig. 2. Evolution of the incidence angle $\theta$ with the distance d between the sample surface and the extraction nose. The values of $\theta$ were calculated by means of SIMION ion optics simulations.

variations of this incidence angle. As a result, the whole range of incidence angles $\theta$ lying between 60° and 90° with respect to the normal to the sample surface is accessible. As the sputtering yield Y is known to reach its maximum value for a given impact energy at an incidence angle $\theta_{max}$ situated between 60° and 80° and to decrease abruptly with increasing $\theta$ between $\theta_{max}$ and 90° [16,17], a large range of sputtering yield values is accessible on the CMS instrument.

For the present work, the CMS $Cs^+$ ion gun was operated at an accelerating energy of 8.5 keV. Since the extraction voltage applied to the sample was 4500 V, the primary beam had an impact energy of 4 keV. As the distance d between the sample surface and the extraction nose can be continuously varied between 1.5 and 2.9 mm, the cited energetic conditions allowed primary impact angles $\theta$ going from 69° to 90° (Fig. 2). The values of $\theta$ were calculated by means of SIMION ion optics simulations [18] taking into account all the geometrical factors, the ion trajectory changes caused by the deflection plates situated in the primary column and destined to position the ion beam on the specimen and finally the electrostatic deflection effects exercised by the polarized sample.

The primary beam was raster-scanned across a rectangular area varying from 300 $\mu$m × 250 $\mu$m to 600 $\mu$m × 250 $\mu$m with increasing incidence angle $\theta$. Typical beam currents lay between 10 and 30 nA. Secondary ions were accepted from a circular area on the sample surface limited to a diameter of 52 $\mu$m, defined by an aperture centered with respect to the scanning area. The mass spectrometer was operated at a mass resolution of $M/\Delta M = 300$ and with an energy band pass $\Delta E = 130$ eV.

On the Cameca IMS 4f [19], analyses were performed at two different sputtering yields. To do so, the primary $Cs^+$ column was operated at an accelerating energy of either 6.5 or 10 keV. As the extraction potential applied to the sample was maintained at 4500 V, the chosen conditions resulted in beam impact angles of 59° and 42° respectively. The beam current ranged from 10 to 20 nA and the beam was raster scanned over an area of 250 $\mu$m × 250 $\mu$m. The mass spectrometer was operated at a mass resolution of $M/\Delta M = 300$ and the energy band pass was maintained at $\Delta E = 130$ eV. The diameter of the analyzed area was set to 33 $\mu$m.

For the present study, depth profiles were performed on the following three identical silicon wafers, which were implanted with two elements each:

1. Si implanted with $^{11}B$ at $10^{16}$ $cm^{-2}$/300 keV and $^{19}F$ at $10^{15}$ $cm^{-2}$/300 keV.
2. Si implanted with $^{24}Mg$ at $10^{15}$ $cm^{-2}$/300 keV and $^{115}In$ at $10^{15}$ $cm^{-2}$/300 keV.
3. Si implanted with $^{32}S$ at $10^{16}$ $cm^{-2}$/300 keV and $^{75}As$ at $10^{15}$ $cm^{-2}$/330 keV.

While fluorine was detected in the $FCs_2^+$ mode because of its high electronegativity, the other elements were analyzed as $MCs^+$ clusters.

At the end of the analyses, the post-bombardment craters were measured with a Tencor P-10 profilometer.

## 3. Results and discussion

For the Mg/In and S/As samples, sputtering yield changes between 8.2 and 12.1 were obtained during the analyses on the CMS machine. The corresponding values of the distance d lay between 1.9 and 2.9 mm. In the case of the B/F sample, measurements were performed at distances ranging from 1.5 to 2.9 mm leading to sputtering yield values between 6.9 and 12.1. For each sample analyses realized at a distance d = 2.5 mm led to the highest sputtering yield.

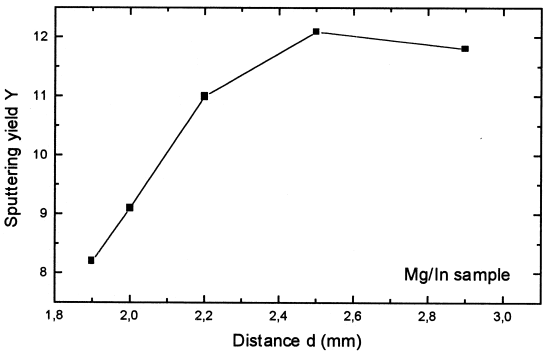


Fig. 3. Variation of the sputtering yield Y against the distance d obtained during experiments on the Mg/In implanted Si sample.

Furthermore, this maximum sputtering yield was found to be 12.1 for any of the three samples. Fig. 3 shows the evolution of the sputtering yield with the distance d obtained on the Mg/In sample.

As for the Cameca IMS 4f, the chosen analysis conditions led to two different sputtering yields. A mean value of 6.4 was found after bombarding the sample at an incidence angle of 42° and an impact energy of 5.5 keV. The reduction of the impact energy to 2 keV and the consequent rise of the incidence angle to 59° resulted in a mean sputtering yield of 7.4.

While the sputtering yield values obtained on the Cameca IMS 4f are situated on the ascending part of the curve tracing the variation of the sputtering yield Y with respect to the impact angle $\theta$ (Fig. 4), the CMS instrument allows to explore the region surrounding the summit of the curve as well as the steep decreasing section on the right-hand side of the summit.

The useful yield of an element M detected as a $MCs_x^+$ cluster is defined

$$UY(MCs_x^+) = \frac{\text{number of detected } MCs_x^+ \text{ ions}}{\text{number of sputtered M atoms}} \quad (1)$$

Considering implanted samples, this definition leads to

$$UY(MCs_x^+) = \frac{\int_0^{t_{final}} I(MCs_x^+, t) \cdot dt}{\varphi \cdot S} \quad (2)$$

where I ($MCs_x^+$, t) represents the intensity of the considered signal as a function of time, $t_{final}$ the duration of the analysis, $\varphi$ the implanted dose of the element M and S the surface of the analyzed area.

For each depth profile, the useful yields of the interesting species were calculated as shown in formula (2) and reported with respect to the corresponding sputtering yield in Fig. 5.

Fig. 5 shows that the useful yields first considerably increase with growing sputtering yields. This enhancement, which takes place until the sputtering yield reaches a value of approximately 9, can be figured to two orders of magnitude for $SCs^+$ and $AsCs^+$ and to one order of magnitude for $BCs^+$, $MgCs^+$, $InCs^+$, and $FCs_2^+$. For sputtering yields larger than 9, two main trends can be distinguished. On the one hand, $MgCs^+$ and $InCs^+$ continue a steady but less pronounced rise. On the other hand $BCs^+$, $SCs^+$, $AsCs^+$, and $FCs_2^+$ exhibit a stabilization followed by a slight final decrease, even though this last behavior is not as clear for $BCs^+$ as for the other three clusters. Interestingly, the useful yield value of $FCs_2^+$ which was calculated after the analysis performed at a distance d of 1.5 mm and which corresponds to a sputtering yield of 6.9 fits perfectly between the two $FCs_2^+$ useful yields obtained on the Cameca IMS 4f. This finding confirms that a direct comparison between the useful yield values derived from analyses performed on the two different instruments is possible. In this context transmission measurements realized on both machines revealed sufficiently close values to make a normalizing unnecessary. These measurements showed furthermore that the transmission factor of the CMS instrument stays constant for distances d ranging from 1.9 to 2.7 mm and that it changes very little (maximum 5%) for smaller respectively larger values of d [15].

To facilitate a comparison between the performances of the CMS on the one side and the Cameca IMS 4f on the other side, the maximum useful yields reached on both instruments for the considered species are compiled in Table 1. Depending on the element, useful yield enhancements ranging from a factor 7 to a factor 80 can be observed between the CMS instrument and the Cameca IMS 4f.

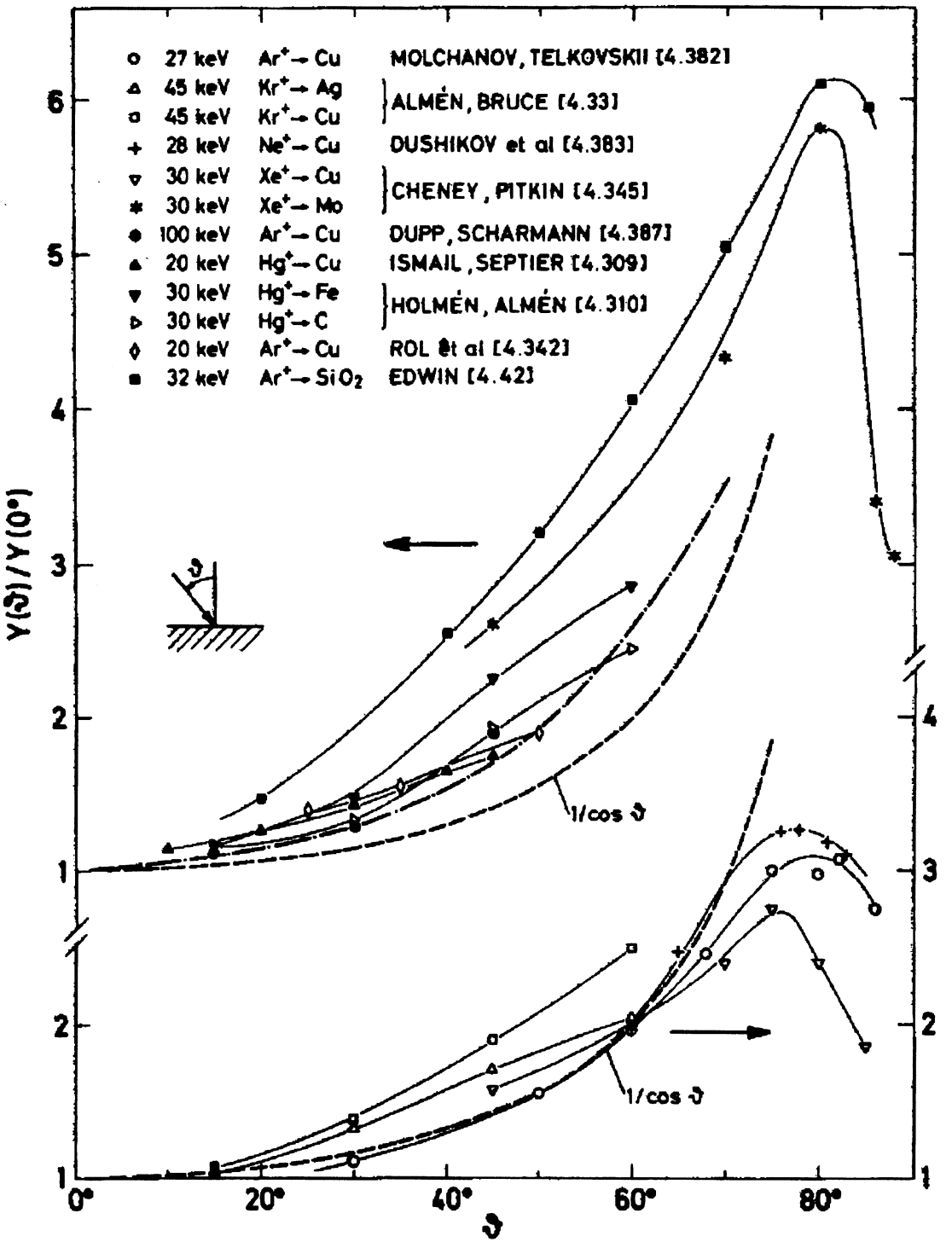


Fig. 4. Heavy-ion sputtering yields in the keV energy region as a function of angle of incidence. Dash-and-dot curve represents the prediction of Sigmund [16]. The dotted curves are drawn only to guide the eye. From [17], with permission of the authors and Springer-Verlag.

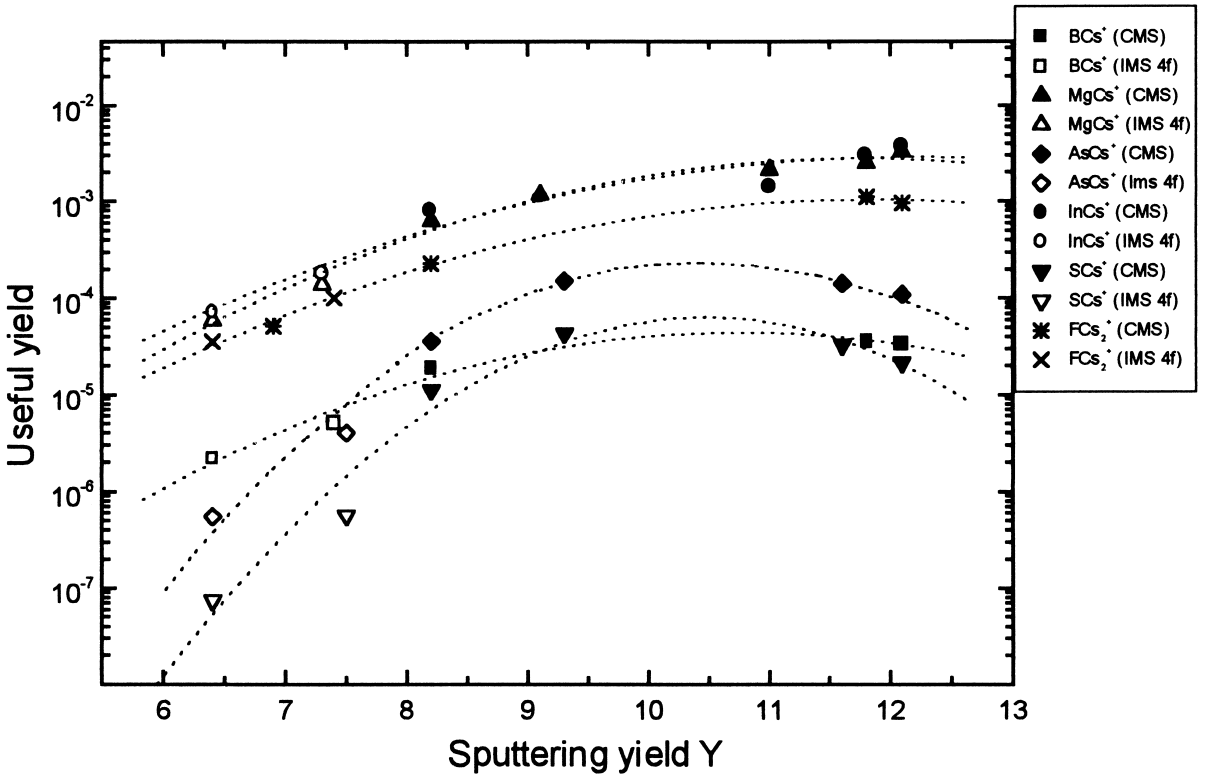


Fig. 5. Compilation of the useful yields determined for the six analyzed species versus the corresponding sputtering yield. While the results obtained on the CMS instrument are represented with plain symbols (for $MCs^+$) or stars (for $FCs_2^+$), those calculated from Cameca IMS 4f analyses are shown with open symbols (for $MCs^+$) or crosses (for $FCs_2^+$). The dotted curves are drawn only to guide the eye.

To discuss the observed evolution of the useful yields with the sputtering yield, some theoretical considerations regarding the formation processes of $MCs_x^+$ clusters have to be made.

$MCs^+$ clusters are formed by an atomic combination of a neutral $M^0$ and a $Cs^+$ ion sputtered in the same single event [3,5,9]

$$M^0 + Cs^+ \rightarrow MCs^+ \quad (3)$$

Consequently, the measured intensity of $MCs^+$ clusters can be expressed by

$$I(MCs^+) = I_p \cdot Y^2 \cdot c_M \cdot c_{Cs} \cdot \beta^+_{Cs} \cdot \gamma_{M^0-Cs^+} \cdot \eta_{MCs^+} \quad (4)$$

where $I_p$ is the primary current, Y is the sputtering yield, $c_M$ gives the surface concentration of the element M, $c_{Cs}$ is the stationary Cs surface concentration, $\beta^+_{Cs}$ represents the ionization probability of a sputtered Cs atom, $\gamma_{M^0-Cs^+}$ is a factor describing the recombination probability between, in this case, the independently sputtered $M^0$ and $Cs^+$ and $\eta_{MCs^+}$ summarizes the geometry, transmission, and detection efficiency of the $MCs^+$ cluster.

Table 1
Comparison between the maximum useful yields obtained on the CMS and the Cameca IMS 4f for the six analysed species

| Species | UY (CMS) | UY (IMS 4f) |
|---|---|---|
| $BCs^+$ | $3{,}6 \times 10^{-5}$ | $5{,}1 \times 10^{-6}$ |
| $MgCs^+$ | $3{,}3 \times 10^{-3}$ | $1{,}4 \times 10^{-4}$ |
| $AsCs^+$ | $1{,}5 \times 10^{-4}$ | $4{,}1 \times 10^{-6}$ |
| $InCs^+$ | $3{,}8 \times 10^{-3}$ | $1{,}8 \times 10^{-4}$ |
| $FCs_2^+$ | $1{,}1 \times 10^{-3}$ | $1{,}0 \times 10^{-4}$ |
| $SCs^+$ | $4{,}4 \times 10^{-5}$ | $5{,}7 \times 10^{-7}$ |

Concerning the $MCs_2^+$ clusters, three different formation processes were proposed [7]

$$M^0 + Cs_2^+ \rightarrow MCs_2^+ \quad (5)$$

$$MCs^0 + Cs^+ \rightarrow MCs_2^+ \quad (6)$$

$$M^- + Cs^+ + Cs^+ \rightarrow MCs_2^+ \quad (7)$$

While the first mechanism seems to be dominating in the case of an electropositive element M, the last two become important for electronegative elements and thus increase their useful yield [7,12]. The $MCs^0$ occurring in the formation process (6) results from the neutralization of a $MCs^+$ ion by electronic capture [20].

The signals corresponding to the $MCs_2^+$ clusters originating from the three considered mechanisms can be written respectively [20,21]

$$\text{for (5): } I(MCs_2^+) = I_p \cdot Y^3 \cdot c_M \cdot c_{Cs}^2 \cdot \beta_{Cs}^+ \cdot (1 - \beta_{Cs}^+) \cdot \gamma_{Cs^0-Cs^+} \cdot \gamma_{M^0-Cs_2^+} \cdot \eta_{MCs_2^+} \quad (8)$$

$$\text{for (6): } I(MCs_2^+) = I_p \cdot Y^3 \cdot c_M \cdot c_{Cs}^2 \cdot \beta_{Cs}^{+2} \cdot \epsilon \cdot \gamma_{M^0-Cs^+} \cdot \gamma_{MCs^0-Cs^+} \cdot \eta_{MCs_2^+} \quad (9)$$

$$\text{for (7): } I(MCs_2^+) = I_p \cdot Y^3 \cdot c_M \cdot c_{Cs}^2 \cdot \beta_M^- \cdot \beta_{Cs}^{+2} \cdot \gamma_{M^--Cs^+-Cs^+} \cdot \eta_{MCs_2^+} \quad (10)$$

In analogy with relation (4), $\gamma$ represents the respective recombination probability and $\eta$ regroups the geometry, transmission, and detection efficiency. The factor $\epsilon$ appearing in reaction (9) denotes the probability of a neutralization of a $MCs^+$ cluster by electronic capture.

The number of sputtered atoms of the element M figuring in formula (1) can be expressed as

$$n(M) = \int_0^{t_{final}} \frac{I_p}{e_0} \cdot Y \cdot c_M(t)\, dt = \frac{I_p}{e_0} \cdot Y \cdot \int_0^{t_{final}} c_M(t)\, dt \quad (11)$$

$e_0$ is the elementary charge, $t_{final}$ is the total sputtering time, and $c_M(t)$ is the concentration of the element M which is a function of depth, and thus of sputtering time t, in the case of implanted atoms.

Considering expressions (4), (8), (9), and (10) regarding the $MCs_x^+$ signals on the one hand and relation (11) concerning the number of sputtered M atoms on the other hand, the following relations for the useful yield can be deduced from formula (1)

$$\text{for (3): } UY(MCs^+) = k_1 \cdot Y \cdot c_{Cs} \cdot \beta_{Cs}^+ \quad (12)$$

$$\text{for (5): } UY(MCs_2^+) = k_2 \cdot Y^2 \cdot c_{Cs}^2 \cdot \beta_{Cs}^+ \cdot (1 - \beta_{Cs}^+) \quad (13)$$

$$\text{for (6): } UY(MCs_2^+) = k_3 \cdot Y^2 \cdot c_{Cs}^2 \cdot \beta_{Cs}^{+2} \cdot \epsilon \quad (14)$$

$$\text{for (7): } UY(MCs_2^+) = k_4 \cdot Y^2 \cdot c_{Cs}^2 \cdot \beta_{Cs}^{+2} \cdot \beta_M^- \quad (15)$$

The factors $k_i$ regroup the recombination probabilities $\gamma$ and the efficiency factors $\eta$ intervening in the respective formation processes and are consequently independent of the stationary Cs surface concentration $c_{Cs}$.

Fig. 6 traces the evolution of the useful yields of the $MCs_x^+$ clusters scaled to $Y^x$ with the stationary Cs surface concentration $c_{Cs}$. This normalization of UY ($MCs_x^+$) with respect to $Y^x$ eliminates the natural increase of the useful yield with a growing sputtering yield and allows to discuss the observed variations in terms of $c_{Cs}$. The quantity $c_{Cs}$ was derived from the sputtering yield Y by applying

$$c_{Cs} = \frac{1}{1 + Y} \quad (16)$$

In analogy to Fig. 5 two main trends can be noticed. The useful yields of $MgCs^+$ and $InCs^+$ decrease on the whole range with growing $c_{Cs}$. This decrease becomes much more pronounced once a $c_{Cs}$ of 0.10 is exceeded. Contrary to these two species, the useful yields of $BCs^+$, $AsCs^+$, $SCs^+$, and $FCs_2^+$ first slightly rise until they reach a maximum value at $c_{Cs}$ values lying between 0.08 and 0.10. Once $c_{Cs}$ grows larger than 0.10, the useful yields of the four species exhibit a steep decrease. Between the mentioned critical value of 0.10 and the maximum value of $c_{Cs}$ reached in the present study, the

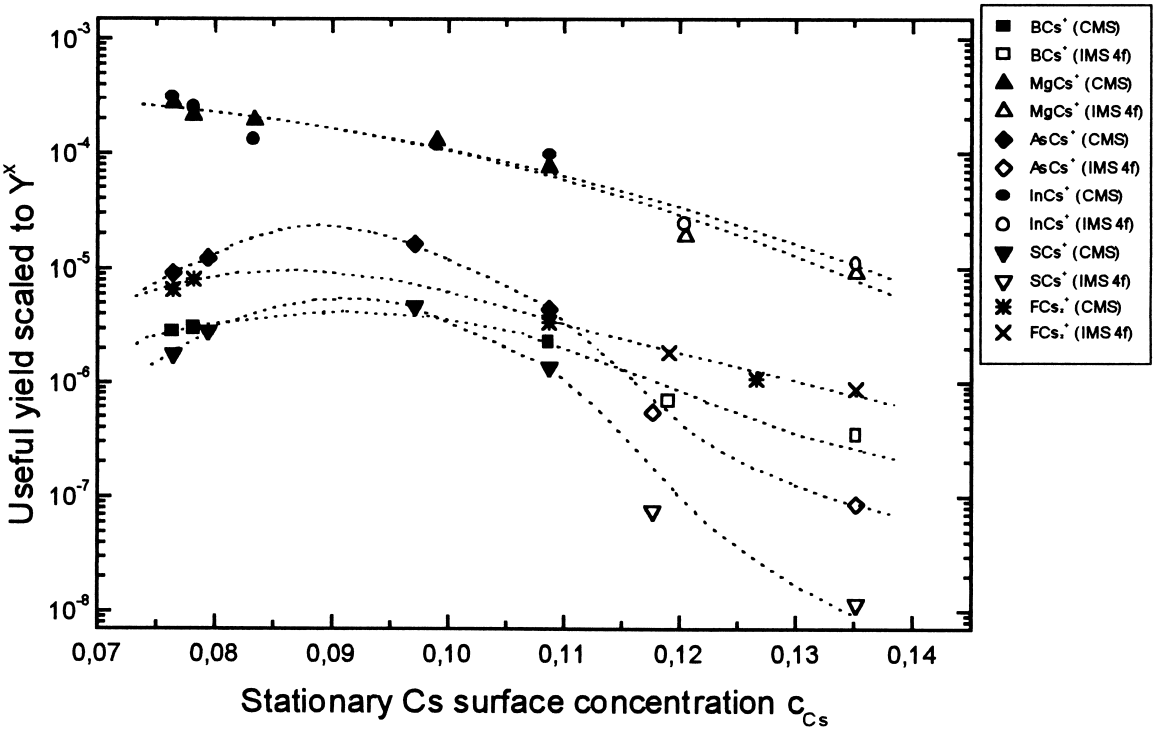


Fig. 6. Variation of the useful yields of the considered $MCs_x^+$ clusters normalized to the respective sputtering yields $Y^x$. Plain symbols (for $MCs^+$) or stars (for $FCs_2^+$) refer to the CMS instrument, open symbols (for $MCs^+$) or crosses (for $FCs_2^+$) stand for the Cameca IMS 4f. The dotted curves are drawn only to guide the eye.

decrease of the useful yields can be figured to two orders of magnitude for $SCs^+$ and $AsCs^+$ and to one order of magnitude for $BCs^+$, $MgCs^+$, $InCs^+$, and $FCs_2^+$. While the analyses on the Cameca IMS 4f led to stationary Cs surface concentrations higher than the mentioned critical value, the experimental conditions chosen on the CMS allowed to lower $c_{Cs}$ below this critical value.

To explain this experimentally observed behavior, the theoretical evolution of the $MCs^+$ and $MCs_2^+$ signals with the stationary Cs surface concentration has been traced in Fig. 7. This graph is valid for samples consisting of an element M to be analyzed and present in any concentration, a variable amount of Cs and any other species (matrix, minors, . . .). The dashed curves show the evolution of the $MCs_x^+$ signals with growing stationary Cs surface concentration if only the influence of $c_{Cs}$ and the concentration of the analyzed species M $c_M$ are considered. The final straight curves are obtained after additionally taking into account the evolution of the ionization probability $\beta^+_{Cs}$ of a sputtered Cs atom. According to the electron tunneling model for secondary ion emission, $\beta^+_{Cs}$ should exhibit an exponential dependence on the work function $\Phi$ of the sample once $\Phi$ becomes lower than a critical value [10,11,22,23]

$$\beta^+_{Cs} \propto \begin{cases} 1, & \text{if } \Phi \geq I \\ \exp\left(-\dfrac{I-\Phi}{\epsilon_0}\right), & \text{if } \Phi < I \end{cases} \quad (17)$$

where I is the ionization potential of Cs and $\epsilon_0$ is an experimental parameter considered to scale with the normal component of the secondary ion's emission velocity [11,24].

The critical value for the work function implies a critical value for the stationary Cs surface concentration, which depends on the considered sample.

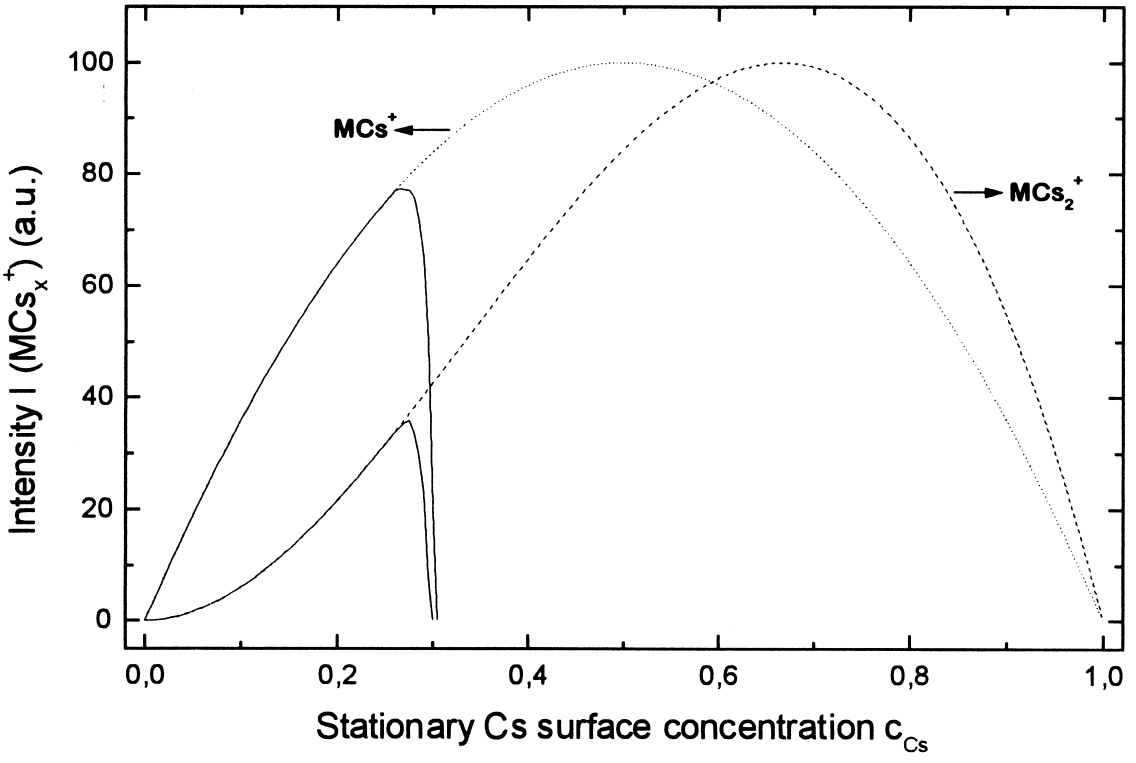


Fig. 7. Theoretical evolution of the $MCs^+$ and $MCs_2^+$ signals with the stationary Cs surface concentration $c_{Cs}$ for any kind of sample. The dashed curves were calculated by considering only the influence of $c_{Cs}$ and the concentration of the analyzed species M $c_M$. The final straight curves are obtained after additionally taking into account the evolution of the ionization probability $\beta^+_{Cs}$ of a sputtered Cs atom. The critical value of $c_{Cs}$ depends on the considered sample and was chosen arbitrarily for the present graph.

In Fig. 6 this signal fall off due to the drastic decrease of $\beta^+_{Cs}$ can be observed for any of the six species. Furthermore, the summit as well as the beginning of the descending part of the curve to the left of the maximum are visible for $BCs^+$, $AsCs^+$, $SCs^+$, and $FCs_2^+$. Consequently, an optimum $c_{Cs}$ value seems to be within reach on the CMS instrument for these four species. In contrast to the precedent clusters, the useful yields of $MgCs^+$ and $InCs^+$, exhibit no summit on the explored $c_{Cs}$ range. Indeed, though the only weak slopes of the respective curves seem to indicate the proximity of the maximum, the $c_{Cs}$ values obtained on the CMS during the present work still seem too large to reach the exact optimum.

An analogous behavior can be observed for the respective curves of two elements coming from the same sample: they evolve in a more or less parallel way and they present their maximum at slightly the same $c_{Cs}$ value. The differences between these optimum $c_{Cs}$ values might be explained by slightly different work functions of the three considered samples even before the incorporation of Cs.

To confirm the results of the present study and to expand it to materials with different work functions, and thus different critical $c_{Cs}$ values, it is indispensable to gain access to a larger range of possible $c_{Cs}$ values, which is the object of present studies on the CMS instrument. The CMS offers this possibility to choose $c_{Cs}$ freely by decoupling the Cs deposition from the primary bombardment conditions. As a matter of fact, neutral Cs can be deposited in adjustable quantities by means of the specially developed Cs evaporator while the sample surface is sputtered with, at present, a $Ga^+$ ion gun. This decoupling

procedure allows to optimize both the $MCs_x^+$ useful yields (by fixing $c_{Cs}$) and other parameters like the depth resolution (by choosing the primary bombardment conditions).

## 4. Conclusion

Useful yields of six different elements implanted in Si wafers and detected in the $MCs_x^+$ modus were determined on the CMS and on the Cameca IMS 4f. On both machines analyses were performed at various sputtering yields by changing the primary bombardment conditions (incidence angle on the CMS and primary energy and incidence angle on the Cameca IMS 4f) in order to monitor the evolution of the useful yields with the stationary Cs surface concentration. Depending on the element, useful yield enhancements ranging from a factor 7 to a factor 80 can be observed between the CMS instrument and the Cameca IMS 4f. This finding can be explained by the fact that compared to the Cameca IMS 4f, the CMS allows to reach lower stationary Cs surface concentrations which are close to the optimum value for the investigated samples.

## References

[1] H.A. Storms, K.F. Brown, J.D. Stein, Anal. Chem. 49 (1977) 2023.
[2] Y. Gao, J. Appl. Phys. 64 (1988) 3760.
[3] H. Gnaser, H. Oechsner, Fresenius J. Anal. Chem. 341 (1991) 54.
[4] K. Wittmaack, Nucl. Instrum. Methods Phys. Res. B 64 (1992) 621.
[5] C.W. Magee, W.L. Harrington, E.M. Botnick, Int. J. Mass Spectrom. Ion Processes 103 (1990) 45.
[6] M.A. Ray, J.E. Baker, C.M. Loxton, J.E. Greene, J. Vac. Sci. Technol. A 6 (1988) 44.
[7] Y. Gao, Y. Marie, F. Saldi, H.-N. Migeon, in Secondary Ion Mass Spectrometry SIMS IX, A. Benninghoven, Y. Nihei, R. Shimizu, H.W. Werner (Eds.), Wiley, Chichester, 1994, p.382.
[8] Y. Gao, Y. Marie, F. Saldi, H.-N. Migeon, in Secondary Ion Mass Spectrometry SIMS IX, A. Benninghoven, Y. Nihei, R. Shimizu, H.W. Werner (Eds.), Wiley, Chichester, 1994, p.406.
[9] T. Mootz, F. Adams, Int. J. Mass Spectrom. Ion Processes 152 (1996) 209.
[10] M.L. Yu, N.D. Lang, Phys. Rev. Lett. 50 (1983) 127.
[11] M.L. Yu, Phys. Rev. B 29 (1984) 2311.
[12] Y. Marie, Y. Gao, F. Saldi, H.-N. Migeon, Surf. Interface Anal. 23 (1995) 38.
[13] T. Kan, K. Mitsukawa, T. Ueyama, M. Takada, T. Yasue, T. Koshikawa, J. Surf. Anal. 5 (1999) 52.
[14] K. Wittmaack, Nucl. Instrum. Methods Phys. Res. B 85 (1994) 374.
[15] T. Mootz, B. Rasser, P. Sudraud, E. Niehuis, T. Wirtz, W. Bieck, H.-N. Migeon, in Secondary Ion Mass Spectrometry SIMS XII, A. Benninghoven, P. Bertrand, H.-N. Migeon, H.W. Werner (Eds.), Elsevier, Amsterdam, 2000, p. 233.
[16] P. Sigmund, Phys. Rev. B 184 (1969) 383.
[17] H.H Andersen, H.L. Bay, in Sputtering by Particle Bombardment I, R. Behrisch (Eds.), Springer, Berlin, 1981, p. 145.
[18] D.A. Dahl, SIMION 3D, Version 6.0.
[19] H.-N. Migeon, C. Le Pipec, J.J. Le Goux, in Secondary Ion Mass Spectrometry SIMS V, A. Benninghoven, R.J. Colton, D.S. Simons, H.W. Werner (Eds.), Springer, Berlin, 1986, p. 155.
[20] T. Mootz, A. Adriaens, F. Adams, Int. J. Mass Spectrom. Ion Processes 156 (1996) 1.
[21] Y. Marie, Doctoral Thesis, Institut National Polytechnique de Lorraine, 1995.
[22] J.K. Nørskov, B.I. Lundqvist, Phys. Rev. B 19 (1979) 5661.
[23] N.D. Lang, Phys. Rev. B 27 (1983) 2019.
[24] H. Gnaser, Phys. Rev. B 54 (1996) 17141.